

Mapping tropical coastal vegetation using JERS-1 and ERS-1 radar data with a decision tree classifier

M. SIMARD*[†], G. DE GRANDI[‡], S. SAATCHI[†] and P. MAYAUX[‡]

[†]Jet Propulsion Laboratory, MS 300–227, 4800 Oak Grove Drive, Pasadena, CA 91109, USA

[‡]Space Application Institute of the European Commission Joint Research Centre, Ispra (VA), Italy

Abstract. The objective of this paper is to investigate the complementarity of JERS-1 and ERS-1 data for mapping coastal tropical regions. We use a decision tree classifier to classify a coastal region of Gabon and describe the feature contribution using the decision tree diagram. The JERS-1 Global Rain Forest Mapping (GRFM) and ERS-1 Central Africa Mosaic Project (CAMP) datasets are used. The result is a land cover map of the west coast of Gabon. The analysis explicitly shows the complementary characteristics of the L- and C-band Synthetic Aperture Radar (SAR) instruments. We demonstrate the usefulness of combined use of L- and C-band data for large area mapping of coastal regions, especially in flooded areas for discrimination of high and low mangroves as well as grasses and tree swamps. The overall classification accuracy increases by 18% over single band classification.

1. Introduction

The objective of this paper is to investigate the complementarity of ERS-1 and JERS-1 Synthetic Aperture Radar (SAR) data for mapping of coastal tropical regions. We use SAR image mosaics constructed in the frame of two continental-scale radar mapping projects: the ERS-1 TREES CAMP (Central Africa Mosaic Project) (Malingreau and Duchossois 1995, De Grandi *et al.* 1999) and JERS-1 GRFM (Global Rain Forest Mapping) (Rosenqvist 1996, De Grandi *et al.* 2000a). The former is a European Commission project executed at the Joint Research Centre (JRC). The latter was initiated by NASDA (National Space Development Agency of Japan) and the JRC (Joint Research Center), Jet Propulsion Laboratory and NASA Alaska SAR Facility acted as the main processing nodes. We focus our study on a coastal area of Gabon.

In moist tropical forest regions, the quasi-permanent cloud cover does not allow for on-demand optical data acquisition of land cover. Thus, in these regions radar data becomes invaluable for mapping land cover (Nezry *et al.* 1993, Luckman *et al.* 1997), hydrography and floods (Ford and Casey 1988, Hess *et al.* 1990, 1995, Kux *et al.* 1993, Kasischke *et al.* 1997). Even if ERS-1 (CVV, C-band vertical polarization) and JERS-1 (LHH, L-band horizontal polarization) are expected to individually provide poor information on tropical forest vegetation species (Kasischke *et al.* 1997,

*e-mail: simard@innu.jpl.nasa.gov

Saatchi *et al.* 1997), they still hold much potential for distinction of low and high biomass as well as wetland mapping (Hess *et al.* 1995, Costa *et al.* 1998). Therefore, this types of data is ideal for tropical coastal mapping. For example, flooded forests can be mapped using L-band data (Hess *et al.* 1995, Kasischke *et al.* 1997), while CVV data performs better for mapping non-wooded wetlands (Kasischke *et al.* 1997), which are in general transparent at L-band. At C-band, flooded forest can be distinguished depending on the canopy structure (e.g. canopy openness, leaf area) (Hess *et al.* 1990, Kasischke *et al.* 1997) and is effective in mapping swamp forest and low land forest in the tropical Africa domain (De Grandi *et al.* 2000b).

We use a decision tree classifier to analyse the data (Breiman *et al.* 1984, Simard *et al.* 2000) because it is independent of data probability distribution. It also allows for efficient use of each input feature in the sense that each feature is used only if it is the best for cleaning a particular group of data samples. A decision tree is a set of hierarchical rules which successively split the data into purer groups. The resulting decision tree diagram is explicit and is useful to assess feature contributions and relations.

In §2 we report on the methodology followed in the compilation of a composite ERS–JERS mosaic. In §3 the thematic classes are described and a brief introduction to the classifier is presented in §4. The analysis, validation and conclusions are discussed in §5.

2. GRFM and CAMP data

We used extracts from the GRFM and CAMP mosaics located on the coast of Gabon between latitude $0^{\circ} 25' 2.8''$ to $3^{\circ} 22' 1.9''$ and longitude $8^{\circ} 28' 40.8''$ to $10^{\circ} 29' 37.8''$. The GRFM mosaic was acquired in November 1996 and the ERS-1 mosaic in August 1994. The GRFM Africa mosaic was derived from these acquisitions by a multi-resolution decomposition, geolocation and tiling of the individual scenes using a direct Mercator projection. Details on the mosaic processing are given in De Grandi *et al.* (2000a). The CAMP mosaic is described in De Grandi *et al.* (1997, 1999). Although the multi-resolution decomposition in the GRFM and CAMP processors generates a pyramid of multi-resolution products, only the so called baseline mosaics with a pixel size of 100m (called framelets) are used in the combined dataset.

The GRFM Africa mosaic was processed using an algorithm which assures an internal geometric consistency at sub-pixel accuracy where each framelet is only allowed to translate and rotate; moreover the addition of external ground control points (GCPs) derived from the World Vector Shoreline database along the coastline gives an absolute geolocation residual mean squared error of 240m. The GRFM dataset was taken as a reference system and the C-band ERS layer composed by rectifying each ERS 100m framelet to the reference mosaic. The rectification procedure uses polynomial warping and a set of tie points measured automatically by cross-correlation between each ERS framelet projected in the Mercator system and the corresponding JERS mosaic subset. Most of the Central Africa basin covered by the ERS mosaic shows very little relief, with some exception for instance in Gabon. In areas of moderate to high relief (from 600 to 1800m) the registration accuracy will however be affected by topography. A number of checks are performed to retain only reliable tie points (windows with a well-defined cross correlation peak). The selected tie-points are used to determine the mapping coefficient by least square (LS) estimation in a polynomial spatial warping procedure. Framelets with poor fitting statistics are flagged in the automatic mosaic compilation procedure and handled by a semi-automatic registration procedure, with interactive tie-point selection. For

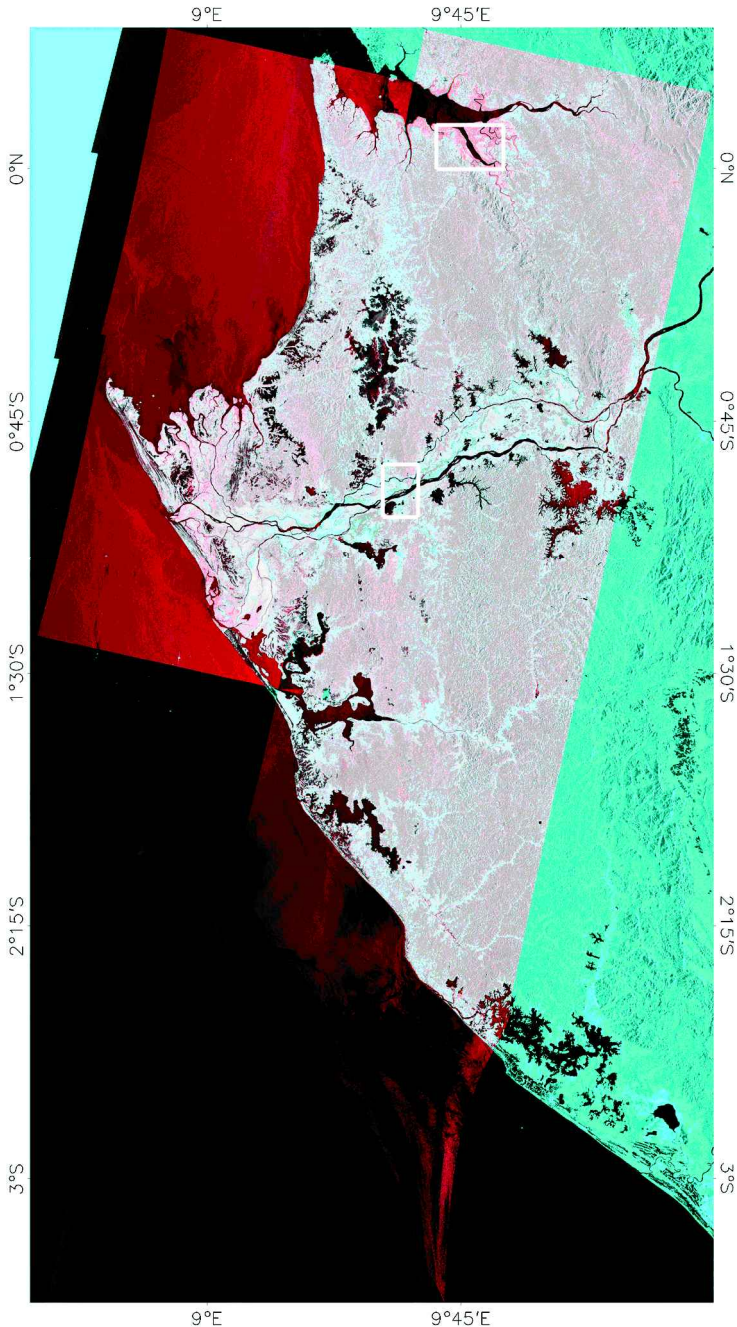


Figure 1. Colour composite image of ERS-1 (red) and JERS-1 (blue). The boxes are shown at full resolution in figure 3. The image covers the area from $0^{\circ} 25' 2.77''\text{N}$ $8^{\circ} 28' 40.81''\text{E}$ (top left corner) to $3^{\circ} 22' 1.88''\text{S}$ $10^{\circ} 29' 37.76''\text{E}$ (bottom right corner).

a more detailed discussion we refer the reader to Mayaux *et al.* (2002). In our case, five ERS-1 framelets (100m resolution images) were co-registered to the GRFM JERS-1 Mosaic. Figure 1 shows the ERS–JERS colour composite image.

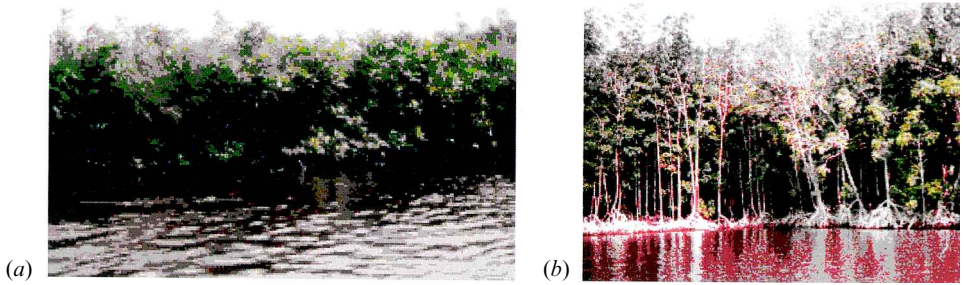


Figure 2. (a) *Rhizophora racemosa* with a thick layer of aerial roots and 20m high canopy. (b) Grasses and papyrus between 2 and 3m height. Some woody shrub is also found in those areas.

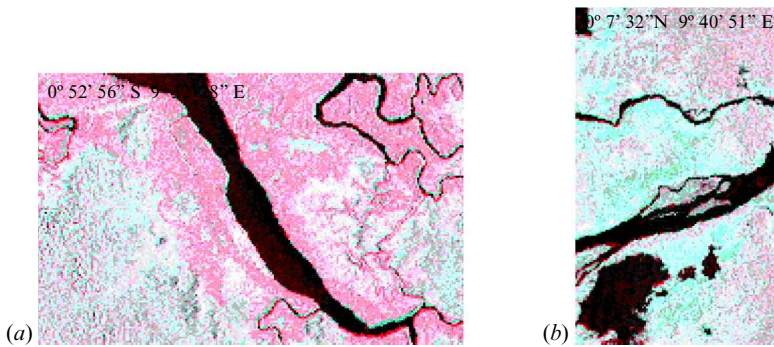


Figure 3. (a) Extract from figure 1 showing the difference in ERS and JERS images for flooded forest which appear yellow (i.e. both high backscatter) and (b) papyrus areas which are blue due to higher relative backscatter in JERS images.

3. Thematic classes

The study area covers a major portion of the Ogooué river basin along the coast of Gabon (figure 1). The land cover types range from grassland and woody savannas to evergreen dense forests. Along the Ogooué basin in the west, the landscape is flat, resulting in areas of very slow drainage and creating wet and sometimes inundated pockets along the river and the coast. The flood plains of the Ogooué river and the mangrove areas along the coast are the main focus of this study. The vegetation types in the region fall in the Guineo-Congolian ecological domain and their ecological significance and definition can be found in several references (Richards 1979, White 1983). In general the definitions found in the literature do not include a detailed geographical location and thus are not suitable for direct implementation in land cover classification from high resolution remote sensing data. In this study, we have used printed land cover maps (OIBT 1998) from *Ministère des eaux et forêts et du reboisement* as a geographical guideline for choosing training areas and validating the derived classified map. The maps were produced by photo-interpretation of aerial and spaceborne data and ground surveys. There is no formal error associated with the map. Moreover our recent field data collection (July 2000) has shown that the classes and their respective training sites were correctly assigned. We have visually chosen 10 dominant vegetation types in the study area for classification. These are:

closed forest, open forest, urban, grass savanna, woody savanna, raffia, flooded forest, grass swamp, low mangrove and high mangrove.

The closed forest class refers to most of the dense humid forest in the region which are considered old and mature secondary forest. There are only few small patches of the primary forest in the eastern part of the study area and south of the city of Lambarene. These are often isolated patches on higher elevation and are predominantly evergreen tall trees with closed canopy. The surrounding old secondary forest contains many deciduous trees. Both JERS-1 and ERS-1 signatures over these forests show almost no variation in texture or backscatter values.

The open forest class consist of young secondary regrowth, intensely logged or disturbed forest, and a mixture of forest and cultivation within the 100m resolution of the image data. The forest has an open canopy with a low density of tall trees. In most cases, the open canopy allows light penetration within the forest which in turn causes the growth of several stages of light-loving herbs in the understory. In optical imagery, these open forests often appear lighter in infrared and therefore distinguished from the primary forest. In L-band radar data, the open forest may appear in a variety of backscatter and texture variations depending on the degree of openness, biomass density level, and the dominance of fast growing single trees (Rignot *et al.* 1997, Saatchi *et al.* 1997, 2000).

The land cover formations of the flood plains along the Ogooué are often over poorly drained soil and can be periodically or frequently flooded. We have identified three vegetation types among these formations. The flooded forest includes all areas with woody vegetation and dense canopy. The grass swamp class includes several herbaceous plants, mainly papyrus, tall grasses, shrubs and some low density woody plants that are waterlogged for most of the year (see figure 2(a)). The Raffia swamps are primarily open canopy dominated by Raffia palms (*Raphia farinifera*) and low vegetation.

The mangrove vegetation types are found along the coasts, rivers and creeks in the intertidal zone where the influence of sea water is significant. Along the coastal area of Gabon, a large area is covered by *Rhizophora racemosa* which have looping aerial roots and downward growing shoots (see figure 2(b)). In the low mangrove areas, mainly *Avicennia germinans* in the form of low scrub or stunted plants with pneumatophores. We also include in the low mangrove class areas of short *Rhizophora harrisonii* (< 5 m).

The urban class is easily distinguished on the SAR images because man made structures act as corner reflectors. The two major urban areas in the image are the city of Libreville and Port-Gentil at the Baie of Cap Lopez.

The savanna classes are uniquely documented on the resulting land cover map (figure 5). Here, we have used two types of savanna vegetation which are primarily based on their woody biomass: grass savanna and woody savanna.

4. Methodology

We use the decision tree method described in Simard *et al.* (2000) which is based on the algorithm of Breiman *et al.* (1984). A decision tree is a hierarchical set of rules. Each rule (or node) splits data into two groups (child nodes) which are purer than the input group (father node). The decision rule maximizes the reduction of impurity measured by the Gini criterion which is defined as follow:

$$1 - \sum_j p^2(j|t) \quad (1)$$

It assigns a sample randomly selected from node t to a thematic class j with probability $p(j|t)$. The sum over j allows for a global decision which emphasizes the purity of the groups rather than the purity of individual classes. For each node in the decision tree including the initial decision, the algorithm searches for the best split by iteratively selecting a threshold on one feature. Then, the reduction of impurity computed for all thresholds on all features are compared and only the best split is selected. Each decision rule is univariate. The result is a hierarchy of decisions which form the decision tree. Thus, using the Gini criterion the decision tree algorithm chooses the best univariate splits for cleaning the input training set group.

There is a final step called pruning that is meant to generalize the decision tree by cutting branches. Each node of the initial decision tree is evaluated in terms of the classification error rate on the training set using a cost-complexity function (Breiman *et al.* 1984). Then, the weakest nodes are successively cut to produce a sequence of smaller decision trees T_k . Finally, the second training dataset is used to test this sequence. The optimum and final decision tree is the one with least overall misclassification rate on the second training set. Each terminal node (following final split) is labelled with the class which has the maximum proportion of sample (memberships) in a given terminal node. For more details, the reader is referred to Breiman *et al.* (1984) or Simard *et al.* (2000).

In addition to the ERS and JERS amplitude images, we computed multiscale texture maps using the wavelet transform (Simard *et al.* 1998). The same transform also provides low resolution images. Each texture map contains a measure of the local spatial variation content of the original image within a scale interval. This type of texture measure can be useful because large scale heterogeneities in the land cover (e.g. degradation, gaps, different targets, etc.) cause image texture (Weishampel *et al.* 1994) that can be used for discrimination of land cover types (Miranda *et al.* 1992, Nezry *et al.* 1993, Oliver and White 1994, Verhoeve 1996, Rignot *et al.* 1997, Yanasse *et al.* 1997, De Grandi *et al.* 2000b). However, image texture measures are also strongly influenced by the spatial resolution and speckle noise. In the case of CAMP and GRFM radar images, the equivalent number of looks is about 60 and therefore, we expect the spatial intensity variation due to land cover structures to become larger with respect to noise induced variation (Simard *et al.* 2000).

Moreover, we use the amplitude ratio feature to enhance differences in the datasets and possibly reduce the decision tree size. For example, if two classes can be separated in the ERS–JERS amplitude feature plane by a diagonal threshold, the mean ratio represents its slope. Otherwise, many splits might be required to obtain the same results. Finally, each class is described by a feature vector containing its label (class) and the following nine features:

- 100 m JERS-1 amplitude data (for reference in figure 4: feature code 0)
- 100 m ERS-1 amplitude data (code 1)
- 200 m JERS-1 amplitude data (code 2)
- 200 m ERS-1 amplitude data (code 3)
- 200 m ERS-1 texture map (code 4)
- 200 m JERS-1 texture map (code 5)
- 400 m ERS-1 texture map (code 6)
- 400 m JERS-1 texture map (code 7)
- 100 m Ratio: JERS/ERS (code 8)

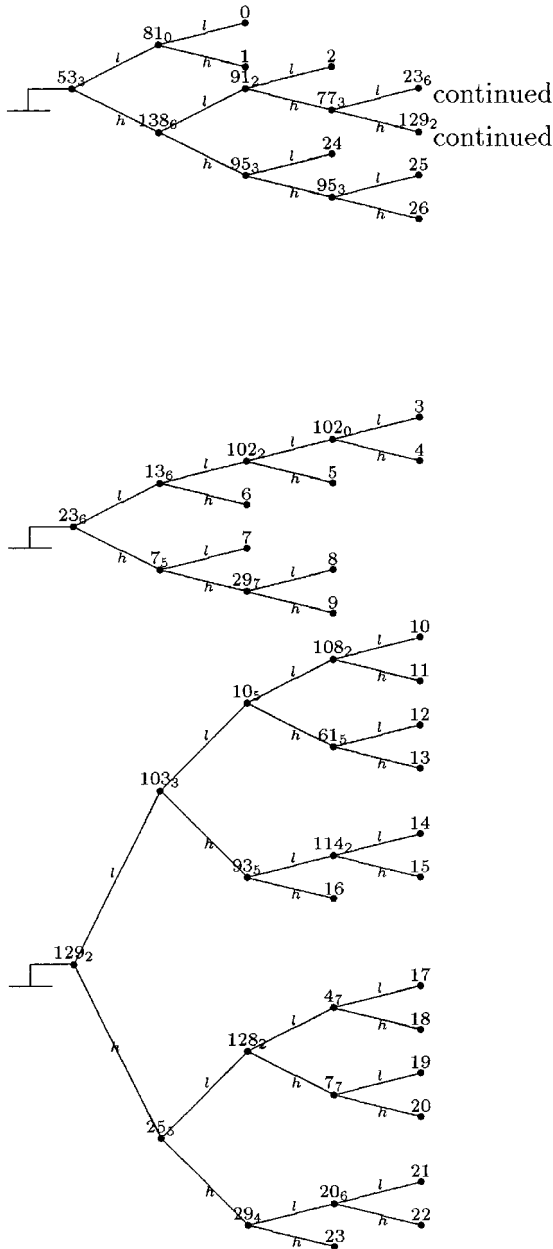


Figure 4. Decision tree classifier. The terminal nodes class labels are inferred from table 1. Each node A_b is characterized by a split A on feature b . The features are in the same order as in the text. Each branch is labelled with l or h meaning lower or higher than threshold A on feature b . The bottom two decision trees are the extensions of the top decision tree.

The decision tree classifier is a supervised method which requires two sets of independent training data which are selected such that intraclass variability is well sampled. The training sets are selected using the land cover map provided by the

Table 1. Class memberships for ERS–JERS classification decision tree in %.

Class node	Forest	Open forest	Urban	Grass savanna	Woody savanna	Raffia	Flooded forest	Swamp	Low mangrove	High mangrove
0	1	0	0	99	0	0	0	0	0	0
1	1	0	0	0	0	0	0	0	0	0
2	2	1	0	2	85	1	0	0	0	3
3	0	0	0	0	0	0	0	8	0	0
4	0	1	0	0	0	0	0	5	0	0
5	0	1	0	0	0	0	0	71	0	0
6	1	1	0	0	0	0	1	7	1	0
7	0	2	0	0	0	0	0	1	0	0
8	6	1	0	0	0	0	0	1	1	0
9	1	0	0	0	0	2	1	1	1	1
10	7	78	0	0	0	0	0	5	0	0
11	35	18	0	0	0	1	7	5	0	0
12	32	1	0	0	0	1	6	0	1	10
13	3	0	0	0	12	1	1	0	1	0
14	3	1	0	0	2	0	0	0	0	87
15	3	1	0	0	0	0	1	0	0	1
16	0	0	0	0	2	0	0	0	7	0
17	1	0	0	0	0	12	9	0	0	0
18	6	0	0	0	0	2	26	0	0	0
19	1	0	0	0	0	56	16	0	0	0
20	1	0	0	0	0	5	11	0	1	0
21	0	0	0	0	0	5	1	1	2	0
22	0	0	0	0	0	2	5	0	1	0
23	3	0	0	0	0	19	22	2	86	0
24	2	0	2	0	0	1	0	0	2	0
25	1	0	0	0	0	0	0	0	0	0
26	0	0	99	0	0	0	0	0	0	0

Ministère des eaux de Forêts et du Reboisement as a geographical guideline and were verified by ground survey. In the GRFM and CAMP data, the intraclass variability is mainly due to the distribution of land cover structures which results in a random distribution of both image radiometry and texture. We sample these spatial variations by using large sampling windows in stationary areas. We must also sample areas near non-stationary points, where more mixed pixels and discontinuities (edges) are present. For example, a grass savanna training area must cover regions lying near and far from class boundaries which have different textural properties because of the edge which is detected by the texture measures. For each class we selected various training sites to build the training sets.

The initial decision tree was grown using randomly 50% of the training samples for each class and the remaining 50% were used for pruning. The final decision tree is shown in figure 4. It has 27 terminal nodes identified from 0 to 26 and it explicitly describes the decision process. The class memberships of its terminal nodes are given in table 1.

5. Analysis and discussion

In this section, we discuss the various feature relationships and contributions as inferred from the decision tree (figure 4). The analysis is performed by identification of the parent splits that were decisive in discriminating classes:

1. The open forest class is discriminated from the closed forest class by the relatively low backscatter in JERS-1 data (terminal nodes 10, 11, 12). The

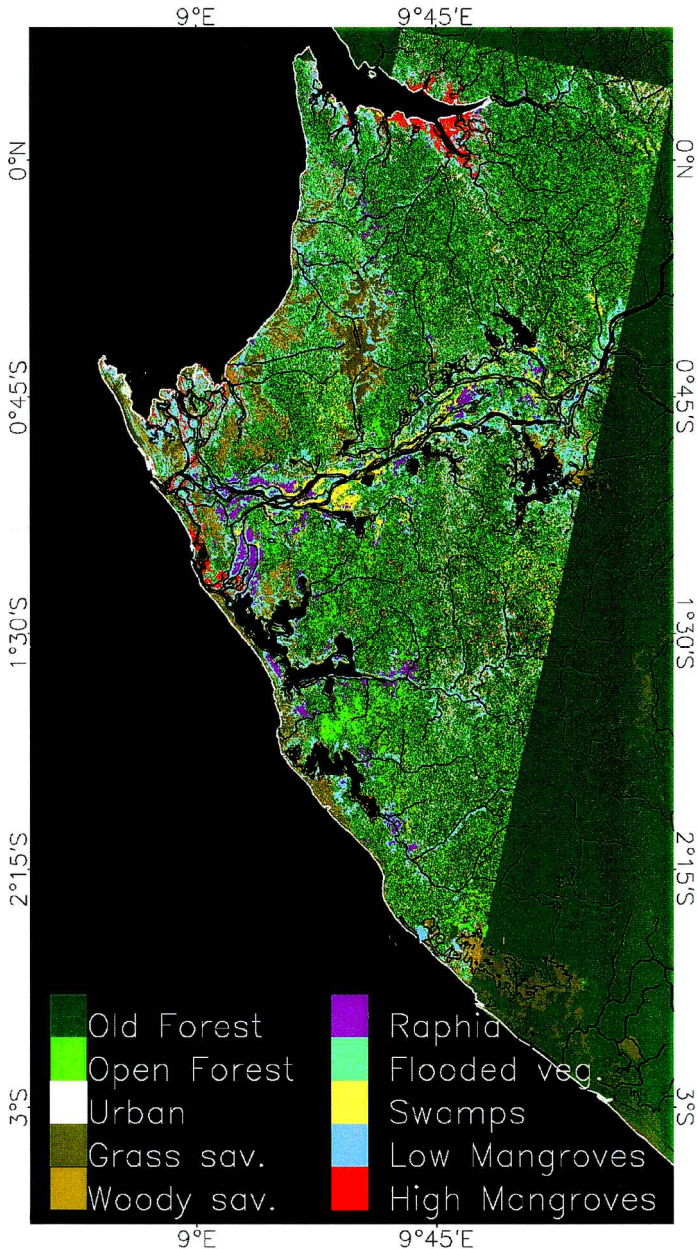


Figure 5. Land cover map of the west of Gabon. The simultaneous use of ERS-1 and JERS-1 allowed for better distinction of high and low flooded vegetation classes.

remaining is discriminated by texture, because the forest training sets included a region with significant relief.

2. The urban area is mainly isolated after a split on ERS-1 texture (terminal node 20). Thus C-band data is more sensitive to urban structures.
3. Woody and grass savannas are mainly in terminal nodes 0 and 2, respectively. In the first case the low backscatter in ERS-1 differentiates grass savannas

Table 2. Confusion matrix for ERS–JERS classification.

Class node	Forest	Open forest	Urban	Grass savanna	Woody savanna	Raffia	Flooded forest	Swamp	Low mangrove	High mangrove
Forest	68	23	0	0	0	0	2	0	3	0
Open forest	3	93	0	0	0	0	0	0	0	2
Urban	0	0	100	0	0	0	0	0	0	0
Grass savanna	0	0	0	90	9	0	0	0	0	0
Woody savanna	1	0	0	0	100	0	0	0	0	0
Raffia	1	0	0	0	0	65	11	0	17	4
Flooded forest	5	0	0	0	0	11	44	0	36	0
Swamp	3	5	0	0	1	0	1	86	0	0
Low mangrove	1	0	0	0	0	0	1	0	96	0
High mangrove	0	0	0	0	0	0	0	0	0	99

Table 3. Confusion matrix for ERS classification.

Class node	Forest	Open forest	Urban	Grass savanna	Woody savanna	Raffia	Flooded forest	Swamp	Low mangrove	High mangrove
Forest	58	21	0	0	12	0	1	0	5	0
Open forest	5	64	0	0	7	21	0	0	0	0
Urban	0	0	100	0	0	0	0	0	0	0
Grass savanna	0	0	0	90	0	0	0	9	0	0
Woody savanna	71	0	0	0	0	0	0	0	28	0
Raffia	0	3	0	0	0	70	0	0	4	21
Flooded forest	1	11	0	2	52	7	3	0	13	6
Swamp	1	3	0	5	1	0	0	85	2	0
Low mangrove	6	0	0	0	4	1	0	0	57	30
High mangrove	0	0	0	0	15	0	0	0	4	79

from woody savannas that have a higher backscatter in C-band data. The split on JERS-1 node (amplitude value of 91 and feature code 2 (91_2)), generally separates savannas (both woody and grass) from higher biomass density vegetation (e.g. forests and flooded classes), which is in agreement with expectations (Kasischke *et al.* 1997).

- The raffia, flooded forest and low mangroves are significantly mixed classes (mainly terminal nodes 19 and 23). The decision tree shows that a large portion of the flooded forest areas will be classified as high mangroves and raffia depending on their spatial pattern (texture). However, JERS texture (node 25_5) contributes to isolate most of the low mangroves from flooded forest and raffia.
- The grass swamps are mainly found in terminal nodes 3–6. It is a split on ERS (node 77_3) which separates grass swamps from forests and flooded vegetation classes. The grass swamps which have a low backscatter in ERS

Table 4. Confusion matrix for JERS classification.

Class node	Forest	Open forest	Urban	Grass savanna	Woody savanna	Raffia	Flooded forest	Swamp	Low mangrove	High mangrove
Forest	56	3	0	0	0	0	0	0	4	34
Open forest	0	72	0	0	0	0	0	5	0	21
Urban	0	0	91	0	0	0	0	0	8	0
Grass savanna	0	0	0	100	0	0	0	0	0	0
Woody savanna	0	0	0	9	90	0	0	0	0	0
Raffia	2	0	0	0	0	55	22	1	17	0
Flooded forest	5	0	2	0	1	33	16	1	38	0
Swamp	10	20	0	0	2	13	0	10	42	0
Low mangrove	0	0	0	0	0	0	0	0	100	0
High mangrove	14	10	0	0	0	0	0	1	0	74

data are then separated from savannas (node 91_2) due to a relatively high backscatter in JERS data (see figure 3). The grass swamps areas are composed mainly of papyrus, tall grasses, shrubs and low woody vegetation which trigger some double bounce effect at L-band, while volume scattering and attenuation occur at C-band within the herbaceous vegetation.

6. The high mangrove class is easily separated from other classes using JERS and ERS together (splits 120_2 and 103_3) because of the low backscatter in JERS-1 LHH data and relatively high backscatter in ERS-1 CVV (see figure 3). For high biomass densities (about 300 tonnes of dry matter per ha), the main scattering mechanism for L- and C-bands is volume scattering. The multiple interaction component at L-band is important (Proisy *et al.* 2000), however, in the present case the strong attenuation and reduced double bounce also occur due to the spatially dense aerial roots which leads to low backscatter (see figure 2(a)). The absence of enhanced backscatter was also observed in other studies for high mangroves (Hess *et al.* 1990). At C-band, scattering saturates in the canopy and thus remains equal for both low and high mangroves.
7. Flooded vegetation classes as a whole (grouping raffia, flooded forest and low mangroves) are easily discriminated from other classes by the strong L-band backscatter, which stems from the double bounce scattering between the water surface and tree structures. A relatively high backscatter is also observed for flooded classes in the CAMP ERS-1 data which is most likely due to some double bounce but also to canopy structure.

Some features were not used in the decision tree. That is the case for the 100m ERS-1 amplitude data, the 200m ERS texture and the 100m JERS data (only used for 1% of closed forest sample in node 1). Their exclusion does not mean the feature are useless, but that other features were better. The consequence is a decrease in the classification spatial resolution. However, this is the compromise to obtain a high overall classification accuracy (Simard *et al.* 2000).

The classified land cover map is presented in figure 5. A water mask was used to segment ocean, lakes and main rivers. To validate the map, an independent test set

was established by selecting new training areas for each class in different geographical areas of the map which also matched with our ground survey. The corresponding confusion matrix for the ERS–JERS classification is shown in table 2. We also computed the confusion matrices for classification using only ERS or JERS which are shown in tables 3 and 4. The overall classification rates are 84, 61 and 66% for ERS–JERS, ERS and JERS, respectively. The Kappa coefficient is 0.8, which is considered very good. In general, the comparison of the confusion matrices for ERS (table 3) and JERS (table 4) show that the off-diagonal elements (errors) are dispersed differently in the matrices. Thus, the combined use of the two datasets is expected to improve results. The ERS misclassification is high for most classes except urban, grass savanna and grass swamps. The mixed classes involve mainly flooded vegetation classes and the woody savanna class. In the JERS case, misclassification is mainly due to commission and omission errors with the low mangrove class, and confusion between the flooded vegetation classes (flooded vegetation, low mangroves and raffia). The grass swamp class is not discriminated. In the combined ERS–JERS classification, the main misclassification occurs between the flooded vegetation classes: raffia and flooded forest with low mangroves and there is also confusion of the closed forest and the open forest classes.

6. Conclusion

We investigated the combined use of JERS-1 GRFM and ERS-1 CAMP (L- and C-band) SAR data for large area mapping of tropical coastal areas. The analysis was performed using a decision tree classifier. It was shown that, due to the complementary characteristics of the two sensors, overall classification results derived from the combined L-band and C-band SAR datasets are improved by 18% with respect to the single band case. Those results could be improved by mainly merging flood classes.

Our ground survey data collected in July 2000 showed correspondence of the image training site with reality. However, the high overall classification accuracy (84%) is applicable to this entire map except for areas with topography in the eastern part of the region where SAR data is not as reliable. The main individual classification accuracy improvement was observed for high mangroves which are indistinguishable using only one dataset. Improvement in the classification accuracy of the forest classes and flooded forest are also significant. Some classes, such as grass swamps which are well classified with ERS only, and woody savannas discriminated with JERS data, are also well classified using both dataset.

The decision tree diagram showed that the use of low resolution data and combined use of ERS and JERS amplitude data were the most useful features. However, new methods for producing full resolution land cover maps using multi-resolution data should be developed to obtain similar classification results.

Acknowledgments

The authors would like to thank NASDA for providing large scale JERS-1 SAR coverage over tropical forest. The work described in this publication was partially carried out by the Jet Propulsion Laboratory, California Institute of Technology, under a contract with the national Aeronautics and Space Administration.

References

BREIMAN, L., FRIEDMAN, J. H., OLSHEN, R. A., and STONE, C. J., 1984, *Classification and Regression Trees* (New York: Chapman and Hall).

- COSTA, M. P. F., DE MORAES NOVO, E. M. L., AHERN, F., MITSUO II, F., MANTOVANI, J. E., BALLESTER, M. V., and PIETSCH, R. W., 1998, The amazon floodplain through radar eyes: Lago grande de monte alegre case study. *Canadian Journal of Remote Sensing*, **24**, 339–349.
- DE GRANDI, F., MALINGREAU, J., LEYSEN, M., SIMARD, M., and MAYAUX, P., 1997, Whither radar global mapping of the tropical forest: new avenues from the TREES ERS-1 central Africa mosaic. *3rd ERS-1 Symposium, Florence, Italy*. <http://florence97.ers-symposium.org/>.
- DE GRANDI, G., MALINGREAU, J., and LEYSEN, M., 1999, The ERS-1 central Africa mosaic: a new perspective in radar remote sensing for the global monitoring of vegetation. *IEEE Transactions on Geoscience and Remote Sensing*, **37**, 1730–1746.
- DE GRANDI, G., MAYAUX, P., RAUSTE, Y., ROSENQVIST, A., SIMARD, M., and SAATCHI, S., 2000a, The global rain forest mapping project JERS-1 radar mosaic of tropical Africa: development and product characterization aspects. *IEEE Transactions on Geoscience and Remote Sensing*, **38**, 2218–2233.
- DE GRANDI, G., MAYAUX, P., MALINGREAU, J. P., ROSENQVIST, A., SAATCHI, S., and SIMARD, M., 2000b, New perspective on global ecosystems from wide-area radar mosaics: flooded forest mapping in the tropics. *International Journal of Remote Sensing*, special issue on *Global and Regional Land Cover Characterization from Satellite Data*, **21**, 1235–1249.
- FORD, J., and CASEY, D., 1988, Shuttle radar mapping with diverse incidence angles in the Rainforest of Borneo. *International Journal of Remote Sensing*, **9**, 927–943.
- HESS, L., MELACK, J. M., and SIMONETT, D., 1990, Radar detection of flooding beneath the forest canopy: a review. *International Journal of Remote Sensing*, **11**, 1313–1325.
- HESS, L. L., MELACK, J. M., FILOSO, S., and WANG, Y., 1995, Delineation of inundated area and vegetation along the amazon floodplain with sir-c synthetic aperture radar. *IEEE Transactions on Geoscience and Remote Sensing*, **33**, 896–903.
- KASISCHKE, E. S., MELACK, J. M., and DOBSON, M. C., 1997, The use of imaging radars for ecological applications—a review. *Remote Sensing of Environment*, **59**, 141–156.
- KUX, H., AHERN, F., RANEY, R., PIETSCH, R., and TITTLE, B., 1993, The contribution of SAREX '92 (south American radar experiment) campaign to the evaluation of natural resources in tropical rain forests: first results from test site acre, sw amazonia, Brazil. *16e Symposium canadien sur la télédétection and 8e congrès de l'Association Québécoise de télédétection* (Québec, Canada: AQT), pp. 53–59.
- LUCKMAN, A., BAKER, J., KUPLICH, T., YANASSE, C., and FRERY, A., 1997, A study of the relationship between radar backscatter and regenerating tropical biomass for spaceborne (SAR) instruments. *Remote Sensing of Environment*, **60**, 1–13.
- MALINGREAU, J.-P., and DUCHOSSOIS, G., 1995, The TREES/ERS-1 SAR'94 project. Earth observation quarterly, ESA, <http://esapub.esrin.esa.it/eqo>, **48**, 1–5.
- MAYAUX, P., GRANDI, G. D., RAUSTE, Y., SIMARD, M., and SAATCHI, S., 2002, Large-scale vegetation maps derived from the combined L-band GRFM and C-band CAMP wide area radar mosaics of Central Africa. *International Journal of Remote Sensing*, **23**, 1261–1282.
- MIRANDA, F., MACDONALD, J., and CARR, J. R., 1992, Application of the semivariogram textural classifier (stc) for vegetation discrimination using sir-b data of Borneo. *International Journal of Remote Sensing*, **13**, 2349–2354.
- NEZRY, E., MOUGIN, E., LOPES, A., GASTELLU-ETCHEGORRY, J., and LAUMONIER, Y., 1993, Tropical mapping with combined visible and SAR spaceborne data. *International Journal of Remote Sensing*, **14**, 2165–2184.
- OLIVER, C., and WHITE, R., 1994, Optimum texture analysis of synthetic aperture radar images. *SPIE Proceedings*, **2230**, 389–398.
- OIBT (ORGANISATION INTERNATIONALE DES BOIS TROPICAUX) and TecSult International for the Ministère des eaux et forêts et du reboisement (March 1998), Formations végétales (1:200000).
- PROISY, C., MOUGIN, E., FROMARD, F., and KARAM, M. A., 2000, Interpretation of polarimetric radar signatures of mangrove forests. *Remote Sensing of Environment*, **71**, 56–66.
- RICHARDS, P. W., 1979, *The Tropical Rain Forest* (Cambridge: Cambridge University Press).

- RIGNOT, E., SALES, W., and SKOLE, D., 1997, Mapping of deforestation and secondary growth in Rondonia, Brazil, using imaging radar and thematic mapper data. *Remote Sensing of Environment*, **59**, 167–179.
- ROSENQVIST, A., 1996, The global rain forest mapping project by JERS-1 SAR. *International Archives of Photogrammetry and Remote Sensing*, Vol. 31, Part B7, pp. 594–598, (Vienna, Austria: ISPRS).
- SAATCHI, S., SOARES, J., and ALVES, D., 1997, Mapping deforestation and land use in Amazon Rainforest by using SIR-C imagery. *Remote Sensing of Environment*, **59**, 191–202.
- SAATCHI, S., NELSON, B., PODEST, E., and HOLT, J., 2000, Mapping land cover types in the Amazon Basin using 1 km JERS-1 mosaic. *International Journal of Remote Sensing*, **21**, 1201–1234.
- SIMARD, M., DE GRANDI, F., and THOMSON, K., 1998, Adaptation of the wavelet transform for the construction of multiscale texture maps of SAR images. *Canadian Journal of Remote Sensing*, **24**, 264–285.
- SIMARD, M., SAATCHI, S., and DE GRANDI, F., 2000, The use of decision tree and multiscale texture for classification of JERS-1 SAR data over tropical forest. *IEEE Transactions on Geoscience and Remote Sensing*, **38**, 2310–2321.
- VERHOEYE, J., 1996, Research on the capabilities of ERS SAR for monitoring of land use changes in the neotropics. Final Report, Laboratory of Forest Management and Spatial Information Techniques, University Gent, Belgium.
- WEISHAMPEL, J., SUN, G., RANSON, K., LEJEUNE, K., and SHUGART, H., 1994, Forest textural properties from simulated microwave backscatter: the influence of spatial resolution. *Remote Sensing of Environment*, **47**, 120–131.
- WHITE, F., 1983, The vegetation of Africa: a description memoir to accompany the UNESCO/AEFTAT/UNSO Vegetation Map of Africa. UNESCO, Paris.
- YANASSE, C. DA C. F., SANT'ANNA, S. J. S., FRERY, A. C., RENNÓ, C. D., SOARES, J. V., and LUCKMAN, A. J., 1997, Exploratory study of the relationship between tropical forest regeneration stages and SIR-C L and C data. *Remote Sensing of Environment*, **59**, 180–190.